NSG-5205

Verification of Mesoscale Objective Analyses of
VAS and Rawinsonde Data Using the March 1982
AVE/VAS Special Network Data

James D. Doyle

and

Thomas T. Warner

Department of Meteorology
The Pennsylvania State University
University Park, PA 16802

January 1987

Abstract

A field program in March 1982 obtained rawinsonde data over a mesoscale
network that had resolution similar to that of the temperature and moisture
data simultaneously obtained from VAS (Visible and infrared spin-scan
radiometer Atmospheric Sounder). This provides a unique opportunity to verify
objective analysis procedures used to combine standard rawinsonde soundings
and VAS soundings of temperature and moisture.

In this study, various combinations of VAS data, conventional rawinsonde
data, and gridded data from the National Weather Service's (NWS) global
analysis, are used in successive-correction and variational objective-analysis
procedures. Analyses are produced for 0000 GMT 7 March 1982, when the VAS
sounding distribution was not greatly limited by the existence of cloud cover.
The successive-correction (SC) procedure is used with VAS data alone,
rawinsonde data alone, and both VAS and rawinsonde data. Variational
techniques are applied in three different ways. In the first, various
combinations of the following constraints are employed in constructing
temperature and humidity analyses: the rawinsonde-data analysis, the
horizontal gradient and Laplacian fields of the VAS-data analysis, and the
vertical gradient fields of the rawinsonde-data analysis. Two weighting
schemes are evaluated for blending the VAS analyses with the rawinsonde
analyses, both on the interior of the VAS data region and on its outer
boundary where it interfaces with the rawinsonde analysis. The second
variational-method application uses VAS precipitable-water gradients and
rawinsonde precipitable-water values to produce humidity analyses. The third
produces a temperature analysis through the use of VAS radiance gradients and
rawinsonde data. These SC and variational analyses were then objectively and

subjectively compared with the AVE/VAS special-network rawinsonde data. The major discernable mesoalpha-scale feature at this time was a cold-air pocket at 500 mb.

When only NWS rawinsonde data were employed in an SC analysis procedure, temperature-error magnitudes at the mesoscale-network sites averaged 0.94°C. The level of maximum error was near 500 mb, where the mesoscale cold-air anomaly caused an average error-magnitude of 1.8°C. When the NWS sounding in the center of the verification network was not used in the analysis, to simulate construction of an analysis within the normal data void between rawinsondes, the three-dimensional temperature error magnitude increased to 1.18°C while the analogous error at 500 mb increased to 2.91°C. The three-dimensional mixing-ratio error, with and without the eliminated sounding, was about .25 g kg^{-1}, with a maximum near 800 mb of .5 g kg^{-1}.

The objective three-dimensional verification statistics show that the use of VAS data to supplement the NWS rawinsonde data significantly decreased the mixing-ratio error magnitude but significantly increased the temperature error. Also, the SC procedure allowed the VAS data to reduce the mixing-ratio error magnitude more than when they were incorporated using any of the variational procedures. Compared to the error associated with the basic NWS global analysis that has not been supplemented with rawinsonde or VAS data, the use of VAS temperature and mixing-ratio data had a positive impact when combined with these global fields. The impact on the moisture field was considerably greater however.

The error statistics for the 500-mb level, where a cold-air bubble provided mesoscale structure over the verification network area, showed trends similar to those seen in the three-dimensional statistics. Two additional

analyses for this level, which used VAS channel-4 radiances directly in a variational procedure, showed promisingly low error. The temperature field first-derivative error was actually less for one of these procedures than for any of the other variational or SC methods. Subjective verification of the temperature fields at this level produced additional insight. First of all, the VAS retrieval data were able to successfully modify the very smooth global analysis to produce a fairly realistic temperature minimum in the verification-network region. Also, the variational procedures were able to successfully blend the rawinsonde and VAS data in the context that the best subjective verification of the cold-pocket structure was produced when both data sources were employed.

1. Introduction

The conventional rawinsonde network is generally inadequate for properly resolving mesoalpha-scale atmospheric structures with sufficient fidelity for use in mesoanalysis and numerical prediction applications. Therefore it is important to make use of other data sources, such as radiometric instruments aboard satellites, to supplement the rawinsonde data. Such an instrument is the Visible/Infrared Spin-Scan Radiometer (VISSR) Atmospheric Sounder (VAS) aboard the Geostationary Operational Environmental Satellites (GOES). VAS is capable of sensing the temperature and moisture structure with a higher temporal and horizontal resolution than can the rawinsonde network, and thus has the potential to improve the quality of mesoscale meteorological analyses. In spite of these potential benefits, VAS data in particular and satellite data in general are often difficult to use in conventional objective-analysis procedures that are designed for use when the data spacing is relatively uniform over the entire analysis domain. Because VAS observations are restricted to cloud-free regions, the irregular density of observations can produce unrealistic gradients and generally make the objective-analysis problem more difficult. Also, even though the temporal and horizontal resolutions of VAS observations are an improvement over those of the conventional rawinsonde network, the vertical resolution is poor. Thus, if the analysis procedure does not heavily weight the vertical gradients from rawinsonde soundings or if the analysis is being performed for a conventional-data-sparse region, the static stabilities may be significantly in error. Because the vertical structure of the initial temperature and moisture variables is very important for numerical forecasts of cloudiness, precipitation and storm-development, this is potentially a serious limitation to use of VAS data sets. A second accuracy-related problem of the VAS data is

that a large-scale bias, relative to rawinsonde data, may exist (Jedlovec, 1984a; Schlatter, 1981). Thus, it is important that an objective analysis procedure be used that capitalizes on gradient information rather than on the magnitude of the VAS data, in order to obtain mesoscale structural information that is potentially available. Because of these problems associated with the blending of data with distinctly different characteristics into an objective analysis, conventional procedures are not likely to be very successful, even though this has not been clearly demonstrated. One reason for this lack of evidence is that rawinsonde data have not been available on the same scale as the VAS data, to allow the accuracy of different objective analysis schemes to be quantitatively determined. However, special high-density rawinsonde data that are co-located with VAS data are available for periods during the 1982 AVE/VAS Ground Truth Field Experiment (Hill and Turner, 1983). We use these data in this study, in which both variational and successive-correction (SC) types of objective analysis procedures are used to combine the VAS data and conventional rawinsonde data for the production of three-dimensional gridded fields that are verified using rawinsonde data from the special mesoscale network.

Various types of objective analysis schemes have been used previously to combine satellite and rawinsonde data in other studies that were less-directly concerned about the analysis process. Some are based on the SC method that was originally developed by Bergthorsson and Doos (1955) and Cressman (1959). There are several examples of studies that have used an SC method to combine radiometric and rawinsonde sounding data. For example, O'lenic (1986) used an SC method to incorporate VAS soundings into the initial conditions of the Limited-area Fine Mesh (LFM) model of the National Weather

Service (NWS). A positive impact on the LFM forecast was found in four cases, however no significant impact was found in two other cases. Wolfson et al. (1985) also used an SC method to assimilate soundings available from two polar-orbiting satellites into the numerical model of the Israel Meteorological Service. A positive impact was found if the satellite data were introduced into meteorologically active regions. These two studies used model forecast accuracy as a gauge of the VAS-data impact and did not focus on alternative objective analysis procedures. In an application of a modified Barnes (1973) SC method, Jedlovec (1984a) showed that objectively analyzed VAS data compared well with subjective analyses of special rawinsonde data for several times on 6 and 7 March 1982 during the AVE/VAS Ground Truth Field Experiment. In another SC analysis of satellite data, Tracton et al. (1980) found that analyses created using only satellite data show less spatial variance in the thermal structure of the atmosphere than is obtained when using other sources such as rawinsonde data.

An alternative to the SC procedure is the variational technique first proposed by Sasaki (1958). It has been applied in many different ways to objectively analyze VAS sounding data. For example, Lewis et al. (1983) used potential-vorticity constraints to adjust the standard rawinsonde-based geopotential analysis to the VAS geopotential analysis for the 6 March 1982 case. In this study, the final analyses were not verified against the special-network observations. Gal-Chen et al. (1985) developed a technique which utilizes the variational method to initialize a numerical model with VAS temperature soundings. A dynamic initialization procedure was used in which horizontal structure was defined by the satellite data while the vertical structure was generated and maintained by the model as the satellite data were

inserted. The poor vertical resolution of the satellite data was compensated for by its higher time resolution. Cram (1982) used horizontal geometric constraints to variationally assimilate VAS data into a global numerical forecast. Since gradient information from VAS is often more reliable than absolute values (Hillger and Vonder Haar, 1977; Chesters et al., 1981), the model first-guess temperature field was constrained to match the observed gradient and Laplacian fields of the satellite data. Similar procedures have also been employed by Lewis (1972), Sasaki and Goerss (1982) and Cram (1985). Cram and Kaplan (1985) also used a variational method to assimilate moisture and temperature gradients into a mesoscale numerical model.

The purpose of this study is to use special mesoscale rawinsonde data that are available from the 1982 AVE/VAS Ground Truth Field Experiment to evaluate the relative accuracy of SC and variational analysis procedures that utilize VAS data and conventional rawinsonde-network soundings of temperature and moisture. Our intent is to 1) compare the skill of the two methods, 2) consider the sensitivity of the performance of each method to the choice of specific parameters or constraints, and 3) determine if the optimal analysis method for this case is dependent on the variable being analyzed. A brief summary of the VAS and a description of the data sets from the 1982 AVE/VAS Ground Truth Field Experiment are provided in Section 2. In Section 3 a description is provided of the synoptic-scale and mesoscale meteorological conditions that prevailed at 0000 GMT 7 March 1982, the time for which the analyses were performed. This is followed in Section 4 by a description of the objective-analysis procedures and in Section 5 by the results of the intercomparisons. Section 6 contains a summary.

2. Data Set Description for 7 March 1982

This section includes discussions of the VAS instrument, the VAS retrieval method, the accuracy of VAS-derived temperature and moisture retrievals, the VAS temperature and moisture retrievals for 6 March 1982, the VAS radiance data for 6 March 1982, and the AVE/VAS special rawinsonde network for this case.

2.1 The VISSR atmospheric sounder

The VISSR Atmospheric Sounder (VAS) was first launched into geostationary orbit aboard GOES-4 in 1980 and is able to provide temperature and moisture soundings on the mesoscale with great temporal resolution. The VAS is a radiometer that senses infrared radiances in 12 thermal-infrared channels, 7 of which are for sensing the temperature, 3 for measuring the water-vapor concentration, and 2 for sensing the surface temperature of the earth and the clouds. The dwell sounding (DS) mode of VAS is used to obtain temperature and moisture profiles. Multiple samples of upwelling radiances are averaged together in the DS mode in order to provide the signal-to-noise ratio required for good sounding quality. Dwell averaging takes place as the VAS spins in a west-to-east direction at 100 revolutions per minute, thus allowing an average to be taken from several spins. The spin budget, or the number of spins that are averaged, is different for each channel, depending upon the noise characteristics. Radiometric noise is further reduced by averaging several fields of view (a horizontal average). However, horizontal resolution is reduced to between 20 and 75 km as a result of this process. The DS mode enables VAS to observe an area with a dimension of about 20 degrees latitude in a period of 30 minutes. After the data are collected, careful selection of the VAS profiles is required because of the influence of low cloud, high

terrain, and irregular surface emissions. For more information about the VAS instrument, refer to Smith (1983) and Chesters et al. (1982).

In obtaining the VAS data used for this study, a dwell imaging (DI) mode was employed. In the DI mode, VAS is able to measure a greater area per unit time than in the DS mode because the number of spins per channel has been reduced and/or some of the channels have been eliminated. This enabled the region of the special rawinsonde network used in this case to be sensed in a short time interval, however the quality of the VAS profiles was not compromised.

2.2 Procedure for VAS temperature and moisture sounding retrieval

There are three VAS sounding retrieval methods: physical, modified physical, and regression (Jedlovec, 1985). When the physical method is applied, a first-guess data set, such as the (LFM) model output, is required. The radiative transfer equation is then solved iteratively. The modified physical scheme uses an analytic solution, after the physical retrievals are obtained, to enhance the vertical structure of the profiles. Smith (1983) describes these two procedures in detail.

The regression procedure uses local rawinsonde and surface data to determine statistical relationships between the structure of the atmosphere and the radiance data. These relationships are then used to derive temperature and moisture profiles where VAS data are not located near rawinsonde sites. VAS soundings in this study were derived using this regression technique. A more detailed discussion of the regression retrieval method can be found in Chesters et al. (1982) and Lee et al. (1983).

The accuracy of the VAS regression retrievals is dependent upon the quality and availability of the conventional data used to "train" the radiance

soundings. Chesters et al. (1982) found that the regression retrievals which used special rawinsonde soundings that were approximately 50 km apart, had smaller residual errors than retrievals which used widely-spaced rawinsondes.

The regression technique makes use of clear-column radiances; thus, VAS retrievals are only possible in cloudless regions. Because the spacing of the conventional rawinsondes is fairly large, it is sometimes necessary to use soundings near the edge of clouds. The dewpoint depression of these rawinsonde observations must be decreased in order to produce better regression correlations with clear-air radiances. Use of these near-cloud data does add a dry bias to the VAS moisture soundings, however it nearly always improves the VAS retrievals (Mostek et al., 1983).

The use of surface temperature and dewpoint-temperature data in the statistical training base greatly improves the quality of the VAS-derived temperature and moisture values in the low-levels. The VAS channel-weighting functions are so broad, that it is difficult to resolve the temperature and moisture structure of the boundary layer without the use of these surface data. Also, surface data enable a proper diurnal effect to be incorporated into the midday VAS retrievals. Otherwise, rawinsonde data that are only available at 1200 GMT and 0000 GMT would frequently cause the surface temperatures, obtained from the VAS window channels, to be too high.

2.3 Characteristics of VAS-derived temperature and moisture sounding retrievals

Chesters et al. (1982), Jedlovec (1984b, 1985), Lee et al. (1983), and Mostek et al. (1983) have investigated the accuracy of VAS-derived temperature and moisture soundings. In these studies, conventional rawinsonde data were used to evaluate the accuracy of the VAS-derived temperature and dewpoint-temperature data from several different dates. There are several error

sources related to VAS temperature and moisture retrievals. Instrument noise and calibration inaccuracy contribute to retrieval errors, however the poor vertical resolution, caused by the broad weighting functions of the infrared channels, is perhaps the most detrimental error. Because of these retrieval problems, Hillger and Vonder Haar (1979) examined the structure of raw satellite radiance data and found much fine-scale information. The structure functions were also similar to those for data provided by mesoscale upper-air networks. However, when inversion techniques are applied, some of this mesoscale structure can be lost (McGinley, personal communication). Chesters et al. (1982) found, when comparing VAS retrievals and rawinsonde data, that errors were greater than the standard deviations. This indicates that gradient information from VAS retrievals may be more accurate and useful than absolute values (Hillger and Vonder Haar, 1977; Chesters et al., 1981). However, even though VAS retrievals generally do identify regions of temperature and moisture gradients, many times the gradients are too weak (Chesters et al., 1982; Jedlovec, 1984b, 1985; Mostek et al., 1983).

2.4 Description of the 6 March 1982 data set

The VAS-derived temperature and dewpoint-temperature data, the VAS radiances and the ground-truth rawinsonde data were supplied by the Goddard Laboratory for Atmospheres of the Goddard Space Flight Center. The retrievals for these data were generated specifically to detect a cold-air bubble which was present in the 400 to 600 mb layer. Minor changes were made to the regression retrieval technique to enhance those channels most sensitive to mid-tropospheric temperature (Dennis Keyser, personal communication).

The VAS temperature and humidity soundings were available for 1730, 2030, and 2330 GMT 6 March 1982, where retrieval sites were approximately 100 km

apart and extended over an area from 27°N to 42°N and 90°W to 107°W. The locations of the sites for 2330 GMT 6 March 1982, the time used for this study, are shown in Fig. 1. There were 153 VAS sounding sites for which data were defined on fifteen pressure levels: 1000, 920, 850, 700, 600, 500, 400, 350, 300, 250, 200, 175, 150, 125, and 100 mb. The data set also included estimates of surface values of pressure, temperature, dewpoint temperature, and surface elevation for these locations. Special rawinsonde data were used for statistical training in the regression retrieval procedure for the 1730 and 2130 GMT VAS data. For the 2330 VAS data retrieval, the standard 0000 GMT rawinsonde data from the 2315 GMT launch were used. The training soundings were located at standard NWS rawinsonde sites, but not the special-network sites.

The radiances from the 12 infrared VAS channels were available for 586 sites distributed at one-half degree latitude and longitude intervals across the VAS sounding region shown in Fig. 1. Each value represented a five pixel by one-line radiance average, where the averaging was intended to reduce radiometric noise. This type of averaging is similar to that used for operational VAS soundings.

The Marshall Space Flight Center and Texas A and M University conducted the field program to provide the ground-truth rawinsonde soundings (Hill and Turner, 1983). Special rawinsonde observations were made over a regional network of NWS sites and a mesoscale network in Texas, at three-hour intervals corresponding to the time of the VAS measurements. The locations of the special observations are shown in Fig. 2. The spacing of the mesoscale-network sites is approximately 125 km. All soundings consisted of geopotential height, temperature, and dewpoint-temperature data defined at 50 mb intervals from the surface to 200 mb. For the time used in this study,

nearly the entire special network area was covered with VAS soundings. The rawinsonde releases occurred approximately 15 minutes before the 2330 VAS observation time.

Further details concerning the AVE/VAS Ground Truth Field Experiment are discussed in Greaves et al. (1982), Jedlovec (1985), and Hill and Turner (1983).

3. Synoptic-scale and mesoscale conditions for 7 March 1982

Figure 3 presents the NMC-analyzed surface conditions for 0000 GMT 7 March 1982 in the special-network region. To the east of this area, a surface low-pressure center was located along the Gulf Coast, with a stationary front extending southward into the Gulf of Mexico to another low-pressure center. A cold front extended from this second low-pressure center, southward across the Gulf of Mexico into Mexico. Showers and thunderstorms were associated with the system. To the northwest of this frontal region, a weak ridge of high pressure was present over the special network. Another cold front extended from a low-pressure system in Canada, through central Missouri into southern Kansas, and across northern Colorado. No precipitation occurred with the front in this region, however scattered clouds were present. To the north of the front, colder and drier air was associated with a high-pressure area centered over North Dakota. A weak surface thermal gradient was positioned across the special network at this time.

Several important synoptic-scale and mesoscale features are seen at 500 mb. Figure 4 is the NMC 500-mb height analysis and shows a trough over eastern Texas. The 500-mb subjective analysis of the temperature, shown in Fig. 5 for the same time, is based on the special-network and the NWS rawinsonde observations. A small bubble of cold air, in the 400 to 600-mb layer, was positioned over the northern part of the region just behind the trough axis. Also, a short-wavelength warm intrusion seems to be present but is poorly defined in the southern part of the special network. The strongest thermal gradient is present to the south and east of the special-network region. The existence of this cold bubble is clearly important to this study because it is a feature that could possibly be resolved by the VAS data. The

synoptic and mesoscale features for this time period are discussed in more detail by Greaves et al. (1982) and Jedlovec (1984b, 1985).

4. The objective analysis procedures

All of the objective analyses were performed on isobaric surfaces spaced 50 mb apart between 1000 mb and 200 mb. The horizontal extent of the analysis domain used in the SC procedures was larger than the one used in the variational procedures, with the smaller matrix being a subset of the larger one. The grid increment was 20 km in both.

4.1 Successive-correction objective analysis procedures

Three of the SC procedures are based on a method developed by Benjamin and Seaman (1985), which is the standard method used in the PSU/NCAR modeling system, and a fourth follows Barnes (1964). Before the analyses were performed, the conventional NWS standard and significant-level rawinsonde data for 0000 GMT 7 March 1982 were logarithmically interpolated to 17 analysis levels (every 50 mb from 1000 to 200 mb). The NMC global analyses were also interpolated to these levels for use as the first-guess field for the rawinsonde-data analysis. In all the SC experiments which used rawinsonde and VAS-derived data, temperature, relative humidity, and the u and v components of the wind were analyzed. Station observations of surface pressure were converted to sea-level pressure, which was also objectively analyzed. The domain for all SC analyses is shown in Fig. 2.

The Benjamin and Seaman procedure uses three kinds of influence functions: circular, elliptical, or curved-elliptical. Only the circular weighting function is used to analyze temperature, since temperature fields rarely exhibit a streaked pattern. For moisture, a pressure-dependent critical wind speed is defined for each analysis level and the elliptical and curved-elliptical weighting functions are used for observations when the local wind speed exceeds this critical value. If this criterion is met, then the streamline radius of curvature at the observation point determines whether the

elliptical or the curved weighting function is used. The curved function is employed when the radius of curvature is less than three times the initial (largest) radius of influence which is 1.6 times the average spacing of the upper-air stations in North America. The radius of influence is reduced to 70% of the previous one for each scan. In the SC analysis of conventional rawinsonde data, four scans were made for all analyzed variables except for relative humidity, which used five scans. This was done because moisture variables frequently exhibit more small-scale structure than do other variables. This standard procedure of the PSU/NCAR modeling system was employed in the successive-correction analysis of the rawinsonde data.

For the SC analysis of the VAS data, the VAS-derived data were interpolated to the 17 analysis levels noted earlier. The VAS dewpoint temperature at each retrieval site and for each analysis level was then converted to relative humidity using the corresponding VAS-derived temperatures. This was done because relative humidity fields are generally smoother than other moisture-variable fields and therefore, in principle, the analysis error should be smaller. The rawinsonde analysis was used as the first-guess field here, but only the VAS data were analyzed. In order to determine the optimal number of scans, the procedure was tested with 4, 5, 6, and 7 scans. As with the analysis of the rawinsonde data, the radius of influence was reduced by 30% for each scan.

The same general procedure was used to incorporate both VAS-derived and rawinsonde data into the same analysis, where no distinction was made between the data sources. The NMC global analysis was used as the first-guess field. Once again, four scans were used for all variables except relative humidity, for which an additional scan was used. Any bias error present in the VAS-derived data was therefore allowed to bias the final analysis. Even

though each individual data point was weighted equally, the final analysis was dominated by the VAS-derived data because there were approximately six times more VAS observations than rawinsonde observations.

The variational procedure that uses VAS radiance gradients, requires a gridded field of radiance data as input. This was obtained from the raw radiance data using the SC procedure developed by Barnes (1964) because very little mesoalpha-scale structure seemed to exist in the fields, and thus it was of special importance that the objective analysis procedure retain any small-amplitude signal. Even though this analysis algorithm is similar to the Cressman type previously described, it was subjectively judged to be less likely to smooth over small-scale features, even though there is no firm evidence to support this assessment. In any case, the results are not likely to be sensitive to the details of the algorithm used—it was still a univariate SC method. A large radius of influence of 1000 km was used for the initial scan to produce a first-guess field. After that, three scans with a radius of influence of 88 km (1.6 times the spacing between the radiance data points) were used.

4.2 Variational objective analysis procedures

Three different variational objective analysis procedures were developed in order to incorporate rawinsonde and VAS data in the same analysis. The first procedure is used to variationally combine rawinsonde data and VAS-derived data in a number of different ways, where the VAS data are in the form of temperature and relative-humidity profiles obtained from the statistical retrieval procedure discussed earlier. In the second procedure, the VAS data were used in the form of the radiances themselves. The third method was similar to the first, except that precipitable-water values

obtained from VAS-derived data were used with rawinsonde precipitable-water values to produce the moisture analyses.

In the first variational procedure used here, a functional similar to that described in Baxter and Goerss (1981) was developed to objectively analyze VAS-derived and rawinsonde temperature and moisture data. The basic functional, in Cartesian coordinates, is

$$J = \int_x \int_y \int_p \{A(V - \bar{V})^2 + B(\frac{\partial V}{\partial x} - \frac{\partial \hat{V}}{\partial x})^2 + C(\frac{\partial V}{\partial y} - \frac{\partial \hat{V}}{\partial y})^2 + D(\frac{\partial^2 V}{\partial x^2} - \frac{\partial^2 \hat{V}}{\partial x^2})^2$$

$$+ E(\frac{\partial^2 V}{\partial y^2} - \frac{\partial^2 \hat{V}}{\partial y^2})^2 + F(\frac{\partial V}{\partial p} - \frac{\partial \bar{V}}{\partial p})^2\} dxdydp \quad , \tag{1}$$

where V is the adjusted, analyzed variable, $\bar{V}$ is the rawinsonde-defined variable, $\hat{V}$ is the VAS-defined variable, and p is the pressure. A, B, C, D, E, and F are weight matrices. The first term in the functional adjusts the analyzed field to the initial rawinsonde field. The second through the fifth terms adjust the analyzed field to the VAS-derived gradients and Laplacians in clear areas and to the rawinsonde-defined gradients and Laplacians elsewhere. The purpose of these four terms is to incorporate mesoscale detail from the satellite data, while not allowing systematic errors to have a negative impact. The final term adjusts the first vertical derivative of the analyzed variable to that of the rawinsonde field, where the purpose is to utilize the good vertical resolution of the rawinsonde data. Thus, the VAS-derived satellite data are allowed to directly add mesoscale information on horizontal structure, but do not <u>directly</u> affect the vertical structure of the analyzed fields. The weight matrices are set to zero around the border of the analysis domain in order to eliminate the boundary terms that result from taking the variation of (1). The weights are set to their full constant value within

the VAS region and are decreased linearly outside the VAS region until they reach a value of zero at the domain boundary. This variable-weighting scheme allows the analyzed variable to be adjusted within the VAS data area, while providing a smooth transition at the edge of the VAS data region. Large gradients in the adjusted field occasionally resulted at the internal data boundaries when this technique was not used. The magnitude of a weight is estimated from the inverse of the expected mean-square difference between the two variables in the particular term in the functional (Lewis and Grayson, 1972). For example, if it is desired that the final adjusted temperatures depart from the rawinsonde-analysis temperatures by 3°C, than A would be set to 3^{-2}. Or, if the VAS-analysis temperature gradient is to depart from the final adjusted temperature gradient by about 10°C/1000 km, B would equal 10^{-4}. Many different combinations of weights are tested here. As noted by Cram and Kaplan (1985), an order of magnitude change in the weight results in only a small change in the product of the variational analysis. In several experiments, weight A was varied not only along the margins of the VAS data region as described above, but also within the VAS region. Near the rawinsonde observations, the final adjusted analysis was constrained very strongly to the rawinsonde analysis, while farther away, the final analysis was given more freedom to depart from the rawinsonde analysis. This procedure recognizes that the high-quality rawinsonde data are most representative of conditions near the observation points. Thus, the final analysis is highly dependent upon the rawinsonde analysis at and near the observations, while the VAS-derived gradients define the mesoscale structure of the final analysis between the rawinsonde observations. The analysis domain for all the variational experiments is shown in Fig. 5.

The second variational procedure was developed to combine conventional rawinsonde temperature fields and VAS <u>radiance</u> data containing finer structures. The basic method is based on the work of John McGinley (personal communication). This method makes use of the satellite radiance data, thus eliminating the need to create temperature profiles using inversion techniques which may remove mesoscale structure. In this simple test of this procedure, where only the 500-mb temperature analysis is verified, only VAS channel-4 radiance data are used.

The functional in two dimensions for a pressure-level p is

$$J = \int_x \int_y \{A(\ln T - \ln \tilde{T})^2 + B(\frac{\partial \ln T}{\partial x} - \frac{\lambda \bar{T}}{c} \frac{\partial \ln R}{\partial x})^2$$

$$+ C(\frac{\partial \ln T}{\partial y} - \frac{\lambda \bar{T}}{c} \frac{\partial \ln R}{\partial y})^2 \} \, dxdy \quad , \tag{2}$$

where T is the analyzed adjusted temperature, $\tilde{T}$ is the rawinsonde temperature, $\bar{T}$ is a representative temperature in a layer, R is a clear-column radiance, c is a constant and A,B, and C are weight matrices. The first term constrains the final adjusted analysis to the rawinsonde analysis while the second and third terms constrain the final analysis to the VAS radiance data. The weight matrices were determined using the procedure described previously.

The third variational procedure was developed to combine rawinsonde-determined precipitable-water values and VAS-derived horizontal gradients of precipitable-water in the analysis of relative-humidity. This is motivated by the concept that the poor vertical resolution of VAS is less

likely to adversely affect the analysis of an integrated quantity such as precipitable water. In the first step, VAS and rawinsonde temperature and moisture data were used to calculate separate precipitable-water analyses. These fields were then used in a variational analysis, where the functional minimized was

$$J = \int_x \int_y \{A(W - \tilde{W})^2 + B(\frac{\partial W}{\partial x} + \frac{\partial \hat{W}}{\partial x})^2 + C(\frac{\partial W}{\partial y} - \frac{\partial \hat{W}}{\partial y})^2\}dxdy \quad . \qquad (3)$$

W is the final adjusted precipitable-water value, $\tilde{W}$ is the rawinsonde precipitable-water value, and $\hat{W}$ is the VAS precipitable-water value. A, B, and C are weight matrices, where a variable-weighting scheme, similar to the one previously described, was used near the perimeter of the VAS data region. The weights within the VAS region were constant. In the second step, the relative-humidity analyses based on the operational rawinsonde data were adjusted to account for the new precipitable-water values. At each grid point, a simple relaxation procedure was used to modify the profiles defined at the 16 analysis levels from 950 to 200 mb, so as to reproduce the variationally analyzed precipitable-water value. For example, if the variationally defined precipitable-water value was slightly greater at a certain grid point than the analogous value based on the rawinsonde analysis, the entire sounding was moistened by the same percent relative humidity at each level until the new precipitable-water value was equivalent to the variationally determined value. Adjusting the moisture profile by adding or subtracting a constant increment of relative humidity at each level is much more realistic than adjusting it by adding or subtracting a constant increment of specific humidity.

5. Experimental Design

Various combinations of VAS-retrieval, VAS radiance, and conventional rawinsonde data were objectively analyzed in order to determine a preferred procedure that would minimize the analysis error. Table 1 summarizes the experiments in terms of the objective analysis scheme, data type, number of scans for the SC experiments, and constraints applied for the variational experiments. The first letter of the experiment code refers to the objective-analysis scheme used, while the next letter(s) indicate the data used. When more than one experiment was performed using the same analysis method and data, an experiment number was added to the end of the code.

5.1 Successive-correction experiments

Two SC analyses were performed using only rawinsonde data. The first-guess field for these experiments was the global NMC analysis. The first analysis, Sr, used the conventional rawinsonde data set without the Stephenville, Texas site, which was located near the center of the special-network (Fig. 2) and near the center of the cold-air pocket at 500 mb. This analysis was performed without this critical observation in order to examine the hypothetical situation where the cold-air pocket was positioned between rawinsonde observations. The entire conventional rawinsonde data set, including the Stephenville site, was used in the Sr_s analysis.

The next four SC analyses used only VAS-derived data and were performed in order to determine the optimal number of analysis scans. The first-guess field for these experiments was the rawinsonde SC analysis from experiment Sr_s. Because the VAS observation spacing is approximately one-third the rawinsonde observation spacing, the possibility existed that more than the normal number of scans (and therefore smaller influence regions) would be

needed to define additional mesoscale structure potentially represented in the VAS data set. Experiments Sv1, Sv2, Sv3, and Sv4, used 4, 5, 6, and 7 scans respectively to analyze the VAS-derived data.

The final SC experiment, Sr_gv, used VAS-retrieval and rawinsonde data, including the Stephenville site. Individual observations from the two data sources were equally weighted by the successive-correction analysis scheme. Because the use of more than four analysis scans in the S_v series caused an increase in the analysis error, only four scans were used here, as in Sr_g.

5.2 Variational objective analysis experiments

A number of variational experiments were performed in which the data input, the constraints, and the weighting schemes differed. Table 2 summarizes the values of the weights used for each variational experiment, where the weights were estimated using the procedure discussed in Section 4. The input fields for the variational scheme were obtained by analyzing rawinsonde and VAS data to the grid using the SC procedures.

Experiment Vgv combined NMC's global analysis and the VAS-derived data. The final adjusted analysis was constrained to the initial global analysis and to the VAS-derived horizontal gradients. Essentially the only synoptic-scale or mesoscale data used here were the VAS-derived data, because the NMC analysis is quite smooth.

The next four experiments, Vrv1, Vrv2, Vrv3, and Vrv4, used VAS-derived data and rawinsonde data without the Stephenville site. The purpose was to determine the impact of each variational constraint upon the final analysis, where we eliminate the Stephenville sounding to determine if the VAS data can define the structure in the data void. In Vrv1, the final analysis was constrained to the rawinsonde analysis and to the VAS-derived horizontal

gradients. For Vrv2, the final analysis was also constrained to the VAS-derived horizontal Laplacians. Vrv3 used the rawinsonde analysis, the VAS-derived horizontal gradients, and the vertical rawinsonde gradients as the constraints. Vrv4 made use of all the constraints in Equation (1).

The next set of four experiments, Vr_sv1, Vr_sv2, Vr_sv3, and Vr_sv4, used rawinsonde data with the Stephenville site and VAS-derived data, where the use of the Stephenville sounding emulates the operational use of all data. Vr_sv1 used the rawinsonde analysis and VAS-derived horizontal gradients as constraints. Vr_sv1 used the rawinsonde analysis and VAS-derived horizontal gradients as constraints. Vr_sv2 used the same constraints as well as the rawinsonde-defined vertical gradients. Vr_sv3 used constraints similar to those of Vr_sv1, but with more weight given to the initial rawinsonde analysis (the value of A was increased). Vr_sv4 also used the same types of constraints as Vr_sv1, however the variable-weighting scheme was applied within the VAS data region.

The final two analyses, Vr_sv_r1 and Vr_sv_r2, both used radiance data and rawinsonde data with the Stephenville site. In both cases, the analysis was constrained to the rawinsonde analysis and to the gradients of the radiance data. They differed in that Vr_sv_r1 weighted the initial rawinsonde analysis more strongly than the other, while in Vr_sv_r2, the variable-weighting scheme was used within the VAS data region. Objective analyses for these two experiments were only created for the 500-mb temperature field because both techniques only used VAS channel-4 radiance data. Also, the most significant meteorological feature in this case is the cold pocket at 500 mb.

5.3 Verification Method

The various analyses were verified based upon the AVE/VAS special-network rawinsonde observations, with the Stephenville, Texas site included. The

spacing between these sites is approximately 125 km, so the drift of the rawinsonde balloons could not be neglected. Therefore, the rawinsonde position was recalculated at each 50-mb level from 950 to 200 mb. For the analysis verification, the data from the objective analyses were interpolated to the special-network observation positions at each level using a bilinear interpolation technique. This was considered to be satisfactory because the analysis-grid mesh size was only 20 km, so interpolation was only required over a short distance. The average absolute error, and the average error were calculated for each level (every 50 mb, from 950 to 200 mb) and for the total three-dimensional analysis grid. The average absolute error is the summation of the absolute value of the error at the verification (observation) points, divided by the number of points. The average error is the summation of the errors at each site, divided by the number of observations; this statistic will of course indicate the bias in the analyses.

The average absolute error in the first horizontal derivative of temperature was also calculated. For each level, first-derivatives were calculated with data from the pairs of observation sites shown in Fig. 6. Then the first-derivatives were calculated using the analysis values that had been interpolated to the observation sites. An average error in percentage form was calculated for every level as well as for all levels combined. Derivative errors were not calculated for a moisture variable because the temperature anomaly at 500-mb was the primary mesoscale feature identifiable in the special-network region.

Subjective comparisons were also made between the verification fields and the analysis fields to evaluate how well the different analysis techniques interpreted some of the specific, observed meteorological features. Because the just-noted fact that the only distinct mesoalpha-scale feature that was

identified by the verification network was the cold-air pool at 500 mb, the
temperature field at this level served as the basis for the subjective
evaluation of the analysis errors.

data in the SC analysis procedure has a positive impact on the moisture-field quality but a negative impact on the temperature-field quality. For example, a comparison of Sr_S and Sv1 shows that VAS reduced the average absolute mixing-ratio error by 29%, but increased the average absolute temperature error by 55%. Sv1, with the same scan-radii as were used for rawinsonde data alone, has a lower average absolute temperature error and first-derivative error than do the other three experiments which utilize additional smaller scans in order to resolve possible mesoscale structure in the VAS data. Note that this result may be slightly misleading because a four-scan successive-correction analysis of rawinsonde data (Sr_S) is used as the first-guess field for these experiments. Because the verification statistics for Sr_S are significantly better than for any experiment in the Sv series, the superior performance of Sv1, compared to others in this series, may be due to the greater influence of the high-quality first-guess field. A clear trend is seen in the temperature-derivative error statistics. Here, the use of smaller scan radii, that is consistent with the higher spatial density of the VAS data, creates a progressively greater error. Ideally this should add mesoscale structure to the analysis, but apparently the error characteristics of the data are magnified by this approach. In contrast, the mixing-ratio error is not sensitive to the number of scans used.

When rawinsonde and VAS data are combined in an SC procedure (Sr_Sv), the results for both temperature and moisture are almost identical to those of experiment Sv1, no doubt because there are approximately six times more VAS-derived soundings than rawinsonde soundings. Thus, as one would expect with typical VAS data densities, the VAS-derived data dominate the analysis and the verification statistics when the two types of data are treated in the same way.

Experiments in the Vrv series utilize different variational constraints to combine VAS data and rawinsonde data. Because the Stephenville sounding is not included in the rawinsonde data set, only VAS data reflect local conditions within the verification network. Of course, the rawinsonde sites surrounding the verification network influence the analysis for the grid points within the verification network. In general, the variational blending of VAS and rawinsonde data produces results similar to when the two data types are combined using the SC procedure--mixing-ratio errors are reduced and temperature errors are increased when VAS data are used, in contrast to the errors when only rawinsonde data are used. Compared to the Sv series of experiments where the SC technique is used to incorporate the VAS data, the variational approach produces a slightly better temperature analysis but a poorer-quality mixing-ratio analysis. Even though there are no great differences in the error statistics within this series of experiments, the temperature field is most accurately analyzed when the horizontal gradient and Laplacian fields of the VAS data are used as constraints, whereas the moisture field verifies better if the vertical gradient field of the rawinsonde data is added as a constraint. Note that the variational constraint based on the vertical derivative of the rawinsonde temperature, causes the temperature-derivative errors in Vrv3 and Vrv4 to be greater than in Vrv1 and Vrv2.

The Vgv analysis variationally combines VAS data with the global analysis of NMC. Even though this global analysis is carefully constructed and is based on rawinsonde data, it is very smooth and could be viewed as having the scale and error characteristics of a good global-model forecast. Thus, Vgv can represent the variational use of VAS data in a large data-void region where the global model forecast is the only other source of "data", while Vrv1

is the analog experiment where rawinsonde data are available. With the global-analysis error used as a reference, the variational use of VAS data in Vgv reduces the mixing-ratio error by 17%, while the variational use of VAS and rawinsonde data in Vrvl reduces the mixing-ratio error by 39%. Analogous reductions in temperature error are 2% and 20%, with VAS data only and with VAS and rawinsonde data, respectively. This interpretation is interesting but is clouded by the fact that VAS data in rawinsonde-data sparse regions (e.g., over the oceans) may not be of the same quality as when rawinsonde data are available. For example, the use of the statistical inversion procedure requires the use of rawinsonde data to determine the regression coefficients. As noted before, a nonstatistical approach is also frequently used however. In the Vr_sv series of experiments, where the Stephenville rawinsonde site is utilized in the analysis, the analysis errors are generally smaller than in the Vrv series.

The vertical variation of the temperature and mixing-ratio error will be examined for three representative experiments. Figure 7 shows the vertical variation of the horizontal average of the temperature error and the temperature-error magnitude for experiments Sr_s, Svl, and Vr_sv4. These plots are based on the analyses produced at 50-mb intervals between 950 mb and 200 mb. The errors for these three experiments are greatest, and also least similar, between 600 and 400 mb, the region of the mesoscale cold-air pocket. Within this layer, a warm bias of 2-3°C exists for Svl. Vr_sv4 shows a smaller bias error of 1-2°C in this same layer. There is very little bias error of more than 0.5-1.0°C in other parts of the sounding for any of the analyses. The average absolute mixing-ratio error and the average mixing-ratio error can be examined in Fig. 8 for the same three analysis procedures. The largest error magnitudes for all three procedures exist in the lower troposphere, with

6. The Analysis Error

6.1 Average error statistics

The average absolute temperature error, average absolute mixing-ratio error, and average absolute first-derivative temperature error were calculated for each experiment shown in Table 1. Error statistics were computed at 16 levels from 950 to 200 mb (every 50 mb) and are summarized in Table 3 as three-dimensional averages.

The two experiments that used only rawinsonde data were based on the SC procedure; one was performed without the Stephenville sounding (Sr) and one with it (Sr_s). The Sr_s error reflects the analysis error that results from use of the operational rawinsonde network when a sounding is in the vicinity of the mesoscale verification grid, while Sr error represents the error that results when the mesoscale verification grid happens to exist in a data-sparse region between operational soundings. The interstation spacing is greater than normal here because an operational sounding has been omitted, but this distance has geographic variations anyhow. Because the Stephenville site is used in the verification data set, it is to be expected that Sr_s verifies better than Sr. The temperature error magnitude is 20% less and the mixing-ratio error magnitude is 8% less in Sr_s than in Sr. The Stephenville sounding provides data in the region of the mesoscale verification network and corrects a bias error that otherwise exists over the network area. Obviously no mesoscale structure is resolvable with this operational synoptic-scale rawinsonde network that provides the data for these analyses. Therefore, the Sr_s error represents remaining uncorrected bias error and the error associated with any unresolved mesoscale structures.

A general comparison of the error associated with the Sv series of analyses with the error from the two Sr analyses shows that the use of VAS

the maximum being near 800-850 mb (Fig. 9a). With the VAS data, the errors
are typically 25% smaller at any particular level. The error shows a dry bias
in the analysis at virtually all levels, with Sr_s having the largest values.
This specific example is contrary to the notion that VAS data have a larger
bias error than do rawinsonde data.

6.2 The 500-mb objective analysis of temperature

As discussed in Section 3, the most significant meteorological feature in
this case is the cold-air pocket at 500 mb. The focus of this section will be
an objective and subjective evaluation of the 500-mb temperature analyses
produced by some of the procedures summarized in Table 1. Table 4 shows the
average error magnitudes and the average first-derivative error magnitudes.
Sr_s has the best overall verification statistics in terms of the error
magnitude. When the Stephenville sounding located near the center of the
cold-air anomaly is withheld from the analysis, the statistics are
significantly worse. It is revealing, but also disconcerting, to note that a
smaller warm bias in the global analysis in the vicinity of the verification
network produces a lower 500-mb temperature error for the global analysis,
than from Sr which uses all the NWS rawinsondes except Stephenville. Sv1 and
Sr_gv do not perform as well as Sr_s and Sr, which is consistent with the
previous observation that the VAS-derived data generally have a negative
impact on the objective statistics for all the temperature analyses, no matter
how the data are used. In Vgv, the VAS data have a similar negative impact on
the global analysis as do the rawinsonde data in Sr. The errors for Vrv1,
Vrv2, Vrv3, Vrv4, Vr_{sv1}, and Vr_{sv2}, which use VAS data in a variational
procedure, are similar to those from Sv1 and Sr_sv which used VAS data in a SC
procedure. A reduction in the average error magnitude is noted when the
Laplacian and the vertical-derivative constraints are used together and
independently.

The final two procedures, Vr_sv_r1 and Vr_sv_r2, which use VAS radiance data and rawinsonde data, produce reasonably good results at this level. The first-derivative temperature error magnitude from both of these procedures is better than from all other experiments. Also, the average error magnitude is lower than in most of the other variational experiments. Figure 9 shows the analysis of the VAS channel-4 radiances and the 500-mb temperature analysis for Vr_sv_r2 which uses the radiances. The temperature field from Vr_sv_r1 is similar. Because there is very little medium-scale horizontal structure to the radiance field, these positive results may have been partially a result of the relatively strong signal from the rawinsonde analysis.

A subjective comparison can be made among the 500-mb temperature analyses to determine if the objective error statistics generally reflect how well the analyses handled individual meteorological features. Figure 10 shows the objective analysis of the verification data and the analyses from Sr_s, $Sv1$, and Vr_sv4. The subjective analysis of 500-mb temperatures from the verification network is found in Fig. 5. Almost all of the variational procedures as well as Sr_sv produce analyses that are similar to those shown in Figs. 10b and c. Sv1 (10b) shows a reasonable structure for the cold-air pocket, with the minimum at the northern end of the elliptical isotherm pattern and a cold-tongue extending southward. However, the temperature minimum is displaced too far to the north. The 500-mb Vgv analysis (not shown), which uses the VAS data alone to modify the smooth NMC global anlaysis, produces a very similar temperature pattern. A temperature minimum of $-28.6°C$ is located over central Oklahoma, with a cold tongue extending to the southwest. Sr_s (10a) and Vr_sv4 (10c), which use the rawinsonde data directly, locate the minimum much better. All of the analyses correctly produce a weak gradient

over northwestern Texas and a stronger gradient in southern Texas. However, none of the procedures capture the actual strength of the gradient in south Texas.

It is noteworthy that Vr_sv4, in one context, successfully blends the VAS-derived data and the rawinsonde data. This analysis (Fig. 10c) correctly defines the location of the center of the cold pocket based on the rawinsonde analysis, and it preserves the correct orientation and aspect ratio of the cold pocket as defined by the VAS data. Other, apparently correct, mesoscale features in the VAS data are retained. For example, the small thermal ridge in the southeastern portion of the special-network area, that is pronounced in the subjective analysis (Fig. 5) and hinted at in the objective analysis (Fig. 10d) can be seen in Sv1 and Vr_sv4 which both use VAS data.

The 500-mb temperature analysis obtained from Vr_sv_r2 (Fig. 9b), which uses VAS radiance data, can be subjectively compared to the analysis from Vr_sv4 (Fig. 10c) in order to determine if the radiance data provide temperature information similar to that of the retrieval soundings. Even though the two analyses generally appear to be quite different, they do have many features in common. The general shapes, orientations, and magnitudes of the cold pockets are similar. Both show a weak thermal ridge in the southeastern corner of the special-network area and a weakening of the temperature gradient in northern Texas. These similarities are to be expected of course, because the VAS radiances, including those of channel 4, were used to create the VAS-derived data set. Therefore, this subjective comparison shows an example of a simple application of the radiance data that produces many of the same benefits obtainable from the use of retrieval soundings.

The rawinsonde analysis, Sr, which pertains to the hypothetical situation in which the center of the cold anomaly is located between rawinsonde

observations, is shown in Fig. 11. By comparison with Sr_s (Fig. 10a), it is

clear the Stephenville sounding has a large impact, especially at this level.

The Sr analysis produces a broad cold area that is weak in amplitude compared

to the cold pocket shown in the verification analysis (Fig. 11d). Thus, if

this mesoalpha-scale feature had actually been located between NWS rawinsonde

observations, the rawinsonde-only analysis could not have properly represented

this cold pocket. However, enough mesoscale structure would have been

available from the VAS data, in the form of radiances or retrieval soundings,

to infer the existence of the temperature minimum and the general shape of the

feature (Figs. 11b).

It is possible to provide some insight into the relative magnitude of the

500-mb analysis errors given in Table 4 by comparing Figs. 9b, 10a-d, and 11.

The position and magnitude of the temperature minimum in Sr_s are better

defined than in $Vr_s v_r 2$, Sv1, $Vr_s v4$ and Sr, even though other characteristics

of the feature are not as realistic. Of the latter four analyses, the

average 500-mb error magnitude of $Vr_s v4$ is less than that of the other three

because the temperatures are lower through the special-network region and are

more in agreement with the verification analysis.

A similar comparison can also explain the first-derivative error

statistics. Experiment $Vr_s v_r 2$ has the lowest first-derivative error because

the position of the weak gradient in the cold pocket verifies better than in

any of the other four analyses. Of the remaining four, Sr_s has the next

smallest first-derivative error for the same reason: the analyzed cold pocket

is positioned closest to the observed cold pocket. In the region of the

observed temperature minimum, a gradient is present in both Sv1 and $Vr_s v4$;

and conversely, where the cold pockets are analyzed, the verification

analysis has a thermal gradient.

Another way of comparing the cold-pocket structure as reproduced by the different analyses is to plot the temperatures along the lines shown in Fig. 10. The middle of the second closed isotherm of the cold-pocket in each analysis is used as the center point for each plot, where the plot is oriented parallel to the major axis of the elliptically shaped isotherm. First note that the temperature profile in Sr_S is not elongated as it correctly is in the other analyses. Also, Sv1 is not nearly cold enough. The temperature minimum in Vr_Sv4 is lower than in Sv1, however the gradient in the southwest is not nearly as large as the analogous gradient shown in the verification-analysis. The length of the cold anomaly in Sv1 and Vr_Sv4 is very close to the observed length shown in the verification analysis. Thus, the VAS analyses represent the shape of the temperature field along this axis better than does the rawinsonde-only analysis. The variational procedure, Vr_Sv4, produces a more realistic gradient at the southwest end of the axis and has the most accurate temperature minimum, compared to the other VAS analyses. Of course this comparison only pertains to the shape of the cold pocket and not the position and orientation which can be compared through Fig. 10.

7. Summary and Conclusions

Variational and successive-correction objective analysis procedures were tested using temperature and humidity data from VAS, from the conventional radiosonde network and from the NMC global analysis. Mesoscale verification data were provided by rawinsonde soundings obtained in Texas during the March 1982 AVE/VAS Ground Truth Field Experiment. The twelve special soundings covered an area that is approximately equal to that normally bounded by four arbitrarily chosen NWS rawinsonde sites. The error associated with each analysis procedure was computed by interpolating from the 20 km analysis grid to the special rawinsonde sites where verification data were available. The verification statistics provide insight into the relative skill of the SC and variational procedures as well as the accuracy of mesoscale structure available from the VAS data in this case. Also, the error statistics from the analyses that did not employ VAS data illustrate the general magnitude of the mesoscale analysis error that results from use of the operational NWS rawinsonde soundings.

When only NWS rawinsonde data were employed in an SC analysis procedure, temperature-error magnitudes at the mesoscale-network sites averaged 0.94°C. The level of maximum error was near 500 mb, where the mesoscale cold-air anomaly caused an average error-magnitude of 1.8°C. When the NWS sounding in the center of the verification network was not used in the analysis, to simulate construction of an analysis within the normal data void between rawinsondes, the three-dimensional temperature error magnitude increased to 1.18°C while the analogous error at 5400 mb increased to 2.91°C. The three-dimensional mixing-ratio error, with and without the eliminated sounding, was about .25 g kg^{-1}, with a maximum near 800 mb of .5 g kg^{-1}.

The objective three-dimensional verification statistics show that the use of VAS data to supplement the NWS rawinsonde data significantly decreased the mixing-ratio error magnitude but significantly increased the temperature error. Also, the SC procedure allowed the VAS data to reduce the mixing-ratio error magnitude more than when they were incorporated using any of the variational procedures. Compared to the error associated with the basic NWS global analysis that has not been supplemented with rawinsonde or VAS data, the use of VAS temperature and mixing-ratio data had a positive impact when combined with these global fields. The impact on the moisture field was considerably greater however.

The error statistics for the 500-mb level, where a cold-air bubble provided mesoscale structure over the verification network area, showed trends similar to those seen in the three-dimensional statistics. Two additional analyses for this level, which used VAS channel-4 radiances directly in a variational procedure, showed promisingly low error. The temperature field first-derivative error was actually less for one of these procedures than for any of the other variational or SC methods. Subjective verification of the temperature fields at this level produced additional insight. First of all, the VAS retrieval data were able to successfully modify the very smooth global analysis to produce a fairly realistic temperature minimum in the verification-network region. Also, the variational procedures were able to successfully blend the rawinsonde and VAS data in the context that the best subjective verification of the cold-pocket structure was produced when both data sources were employed.

Acknowledgements

Table 1 Description of experiments.

Experiment Code Number	Objective Analysis Type	Data	Number of Scans/Constraints
Sr	Suc. Cor.	r	4
Sr_s	Suc. Cor.	r_s	4
$Sv1$	Suc. Cor.	v	4
$Sv2$	Suc. Cor.	v	5
$Sv3$	Suc. Cor.	v	6
$Sv4$	Suc. Cor.	v	7
Sr_sv	Suc. Cor	r_s,v	4
Vgv	Var.	g,v	g,G_h
$Vrv1$	Var.	r,v	r,G_h
$Vrv2$	Var.	r,v	r,G_h,L_h
$Vrv3$	Var.	r,v	r,G_h,G_v
$Vrv4$	Var.	r,v	r,G_h,L_h,G_v
$Vrv5$	Var.	r,v	r,G_h
Vr_sv1	Var.	r_s,v	r_s,G_h
Vr_sv2	Var.	r_s,v	r_s,G_h,G_v
Vr_sV3	Var.	r_s,v	r_s,G_h
Vr_sv4^*	Var.	r_s,v	r_s,G_h
Vr_sv_r1	Var.	r_s,v_r	r_s,G_h
$Vr_sv_r2^*$	Var.	r_s,v_r	r_s,G_h

*variable-weighting scheme within the VAS data region

S — successive correction $\qquad$ V — variational

r — rawinsonde (without Stephenville site) $\qquad$ v — VAS

r_s — rawinsonde (with Stephenville site) $\qquad$ v_r — VAS radiance

g — NMC Global Analysis $\qquad$ G_h — horizontal gradient

L_h — horizontal Laplacian $\qquad$ G_v — vertical gradient

Table 2 Values of weights used in the variational objective-analysis experiments.

Exp. Code No.	Variable Analyzed	Functional Equation	A	B	C	D	E	F
Vgv	T	1	0.1	10^{10}	10^{10}	—	—	—
	RH	1	0.01	10^{9}	10^{9}	—	—	—
Vrv1	T	1	0.1	10^{10}	10^{10}	—	—	—
	RH	1	0.01	10^{9}	10^{9}	—	—	—
Vrv2	T	1	0.1	10^{10}	10^{10}	10^{20}	10^{20}	—
	RH	1	0.01	10^{9}	10^{9}	10^{18}	10^{20}	—
Vrv3	T	1	0.1	10^{10}	10^{10}	—	—	10^{4}
	RH	1	0.01	10^{9}	10^{9}	—	—	10^{2}
Vrv4	T	1	0.1	10^{10}	10^{10}	10^{20}	10^{20}	10^{4}
	RW	1	0.01	10^{9}	10^{9}	10^{18}	10^{18}	10^{2}
Vrv5	PW	3	0.1	10^{11}	10^{11}	—	—	—
$Vr_s v1$	T	1	0.1	10^{10}	10^{10}	—	—	—
	RH	1	0.01	10^{9}	10^{9}	—	—	—
$Vr_s v2$	T	1	0.1	10^{10}	10^{10}	—	—	—
	RH	1	0.01	10^{9}	10^{9}	—	—	—
$Vr_s v3$	T	1	1.0	10^{10}	10^{10}	—	—	—
	RH	1	0.04	10^{9}	10^{9}	—	—	—
$Vr_s v4$	T	1	*	10^{10}	10^{10}	—	—	—
	RG	1	*	10^{9}	10^{9}	—	—	—
$Vr_s vr1$	lnT	2	7.9×10^{4}	8×10^{14}	8×10^{14}	—	—	—
$Vr_s vr2$	lnT	2	*	8×10^{14}	8×10^{14}	—	—	—

*variable-weight scheme within the VAS data region used

T — temperature
RH — relative humidity
PW — precipitable water values

Table 3. Three-dimensional averages of the absolute temperature and mixing-ratio errors, and the average absolute first-derivative temperature error.

Experiment Code Number	Average Absolute Mixing-Ratio Error (g kg^{-1})	Average Absolute Temperature Error (°C)	Average Absolute First-Derivative Temperature Error (%)
Sr_s	.240	0.94	75.8
Sr	.262	1.18	79.0
Svl	.169	1.44	88.8
Sv2	.170	1.50	97.4
Sv3	.169	1.57	107.7
Sv4	.169	1.60	113.3
Sr_sv	.165	1.40	89.6
Vgv	.286	1.75	88.7
Vrvl	.202	1.43	85.4
Vrv2	.203	1.33	85.7
Vrv3	.186	1.41	88.2
Vrv4	.189	1.39	88.4
Vrv5	.221	---	---
Vr_svl	.194	1.30	85.0
Vr_sv2	.183	1.37	87.9
Vr_sv3	.213	1.02	79.2
Vr_sv4	.201	1.08	82.3
Global Analysis	.331	1.79	86.1

Table 4 Average error magnitude and the average first-derivative error magnitude for the 500-mb temperature.

Experiment Code Number	Average Absolute 500-mb Temperature Error (°C)	Average Absolute First Derivative 500-mb Temperature Error (%)
Sr_s	1.83	98
Sr	2.91	106
$Sv1$	3.21	110
Sr_sv	3.10	112
Vgv	3.01	109
$Vrv1$	3.41	106
$Vrv2$	3.15	106
$Vrv3$	3.12	109
$Vrv4$	3.07	109
Vr_sv1	2.95	104
Vr_sv2	3.01	108
Vr_sv3	2.35	99
Vr_sv4	2.49	103
Vr_sv_r1	2.27	95
Vr_sv_r2	2.78	97
Global analysis	2.88	112

References

Barnes, S.L., 1964: A technique for maximizing details in numerical weather map analysis. J. Appl. Meteor., 3, 396-409.

Barnes, S.L., 1973: Mesoscale objective map analysis using weighted time-series observations. NOAA Tech. Memo. ERL NSSL-62, 60 pp. [NTIC COM-73-10781].

Baxter, T. and J.S. Goerss, 1981: Variational high-resolution meteorological analysis. Final Report by Atmospheric Research Corporation, Norman, OK to NASA Goddard Space Flight Center Contracat NAS-5-26206, 168 pp.

Benjamin, S.G. and N.L. Seaman, 1985: A simple scheme for objective analyses in curved flow. Mon. Wea. Rev., 113, 1184-1198.

Bergthórssen, and B.R. Döös, 1955: Numerical weather map analysis. Tellus, 7, 329-340.

Chesters, D., L.W. Uccellini, H. Montgomery, A. Mostek and W. Robinson, 1981: Assessment of the first radiances received from the VISSR Atmospheric Sounder (VAS) instrument. NASA Tech. Memo. 83827, 124 pp. [NTS-82N19730].

Chesters, D., L.W. Uccellini and A. Mostek, 1982: VISSR Atmospheric Sounder (VAS) simulation experiment for a severe storm environment. Mon. Wea. Rev., 110, 198-216.

Cram, J.M., 1982: A Variational Scheme for Assimilation of Satellite-Derived Temperatures. M.S. Thesis, University of Oklahoma, 134 pp.

Cram, J.M., 1985: Variational assimilation of asynoptic data on 10 April 1979. Preprints, Seventh Conf. on Numerical Weather Prediction, Montreal, Canada, Amer. Meteor. Soc., 69-26.

Cram, J.M. and M.L. Kaplan, 1985: Variational assimilation of VAS data into a mesoscale model; assimilation method and sensitivity experiments. Mon. Wea. Rev., 113, 467-484.

Cressman, G.P., 1959: An operational objective analysis system. Mon. Wea. Rev., 87, 367-374.

Gal-Chen, T., B. Schmidt and L.W. Uccellini, 1985: An initialization procedure for assimilating geostationary satellite data into numerical weather prediction models. Preprints, Seventh Conf. on Numerical Weather Prediction, Montreal, Canada, Amer. Meteor. Soc., 61-68.

Greaves, J., H. Montgomery, L.W. Uccellini and D. Endres, 1982: The 1982 AVE/VAS Ground Truth Field Experiment: Satellite data acquisition summary and preliminary meteorological overview. NASA Report X-903-82-17, 27 pp.

Hill, C.K. and R.E. Turner, 1983: NASA's AVE/VAS program. Bull. Amer. Meteor. Soc., 64, 796-797.

Hillger, D.W. and T.H. Vonder Haar, 1977: Deriving mesoscale temperature and moisture fields from satellite radiance measurements over the United States. J. Appl. Meteor., 16, 715-726.

Hillger, D.W. and T.H. Vonder Haar, 1979: An analysis of satellite infrared soundings at the mesoscale using statistical structure and correlation functions. Mon. Wea. Rev., 36, 287-305.

Jedlovec, G.J., 1985: An evaluation and comparison of vertical profile data from the VISSR Atmospheric Sounder (VAS). NASA Tech. Paper 2425, 33 pp.

Jedlovec, G.J., 1984a: Application of VISSR Atmospheric Sounder (VAS) data in weather analysis. Preprints, Tenth Conf. on Weather Forecasting and Analysis, Clearwater Beach, Amer. Meteor. Soc., 350-357.

Jedlovec, G.J., 1984b: A statistical evaluation and comparison of VISSR
    Atmospheric Sounder (VAS) data and corresponding rawinsonde measurements.
    NASA Tech. Memo. 82575, 11 pp.

Lee, T., D. Chesters and A. Mostek, 1983: The impact of conventional surface
    data upon VAS regression retrievals in the lower troposphpere. J.
    Climate Appl. Meteor., 22, 1853-1873.

Lewis, J.M., 1972: An operational upper air analysis using the variational
    method. Tellus, 6, 514-530.

Lewis, J.M. and T.H. Grayson, 1972: The adjustment of surface wind and
    pressure by Sasaki's variational matching technique. J. Appl. Meteor.,
    11, 586-597.

Lewis, J.M., C.M. Hayden and A.J. Schreiner, 1983: Adjustment of VAS and RAOB
    geopotential analysis using quasi-geostrophic constraints. Mon. Wea.
    Rev., 111, 2058-2067.

Mostek, A., D.A. Keyser, T. Lee and L.W. Uccellini, 1983: Remote retrievals
    for the 6 March 1982 AVE/VAS special network. Goddard Laboratory for
    Atmospheric Sciences, 15 pp.

O'lenic, E.A., 1986: The effect of VISSR atmospheric sounder data on some
    LFM analyses and forecasts. Mon. Wea. Rev., 114, 1832-1846.

Sasaki, Y., 1958: An objective analysis based on the variational method. J.
    Meteor. Soc. Japan, 36, 77-88.

Sasaki, Y. and J. S. Goerss, 1982: Satellite data assimilation using NASA
    data systems test 6 observations. Mon. Wea. Rev., 110, 1635-1644.

Schlatter, T.W., 1981: An assessment of operational TIROS-N temperature
    retrievals over the United States. Mon. Wea. Rev., 109, 110-119.

Smith, W.L., 1983: The retrieval of atmospheric profiles from VAS geo-
    stationary radiance observations. J. Atmos. Sci., 40, 2025-2035.

Tracton, M.S., A.J. Desmarais, R.J. van Haaren and R.D. McPherson, 1980: The impact of satellite soundings upon the National Meteorological Center's analysis and forecast system – the Data Systems Tests results. Mon. Wea. Rev., 108, 543-586.

Wolfson, N., A. Thomasell, A. Gruber and G. Ohring, 1985: The impact of satellite sounding data on the systematic error of a numerical weather prediction model. Mon. Wea. Rev., 113, 1031-1049.

Figure 9   The results of experiments Vr_sv_r2 using rawinsonde data and VAS
             radiance data.

   a.   Analysis of VAS channel-4 raw radiances (ergs). The contour
        interval is 1 erg.

   b.   The 500-mb temperature analysis (°C) from experiment Vr_sv_r2.
        The contour interval is 1°C. The dashed contour in the region
        of the cold pocket is plotted at a 0.5°C interval.

Figure 10   The 500-mb temperature analysis (°C) for Sr_s(a), Srl (b), and
             Vr_sv4 (c) and the verification field (d). The contour interval
             is 1°C, however the dashed contours in the region of the cold
             pocket are plotted every 0.5°C. One-dimensional temperature plots
             were taken along the lines indicated in each analysis.

Figure 11   The 500-mb temperature analysis (°C) from experiment Sr. The
             contour interval is 1°C. The dashed contours in the region of the
             cold pocket are plotted every 0.5°C.

Figure 12   The one-dimensional 500-mb temperature plots for experiments Sr_s,
             Svl, Vr_sv4, and the analysis of the special-network data and the
             NWS rawinsonde data. The lines along which the data are plotted
             are shown in Fig. 11.
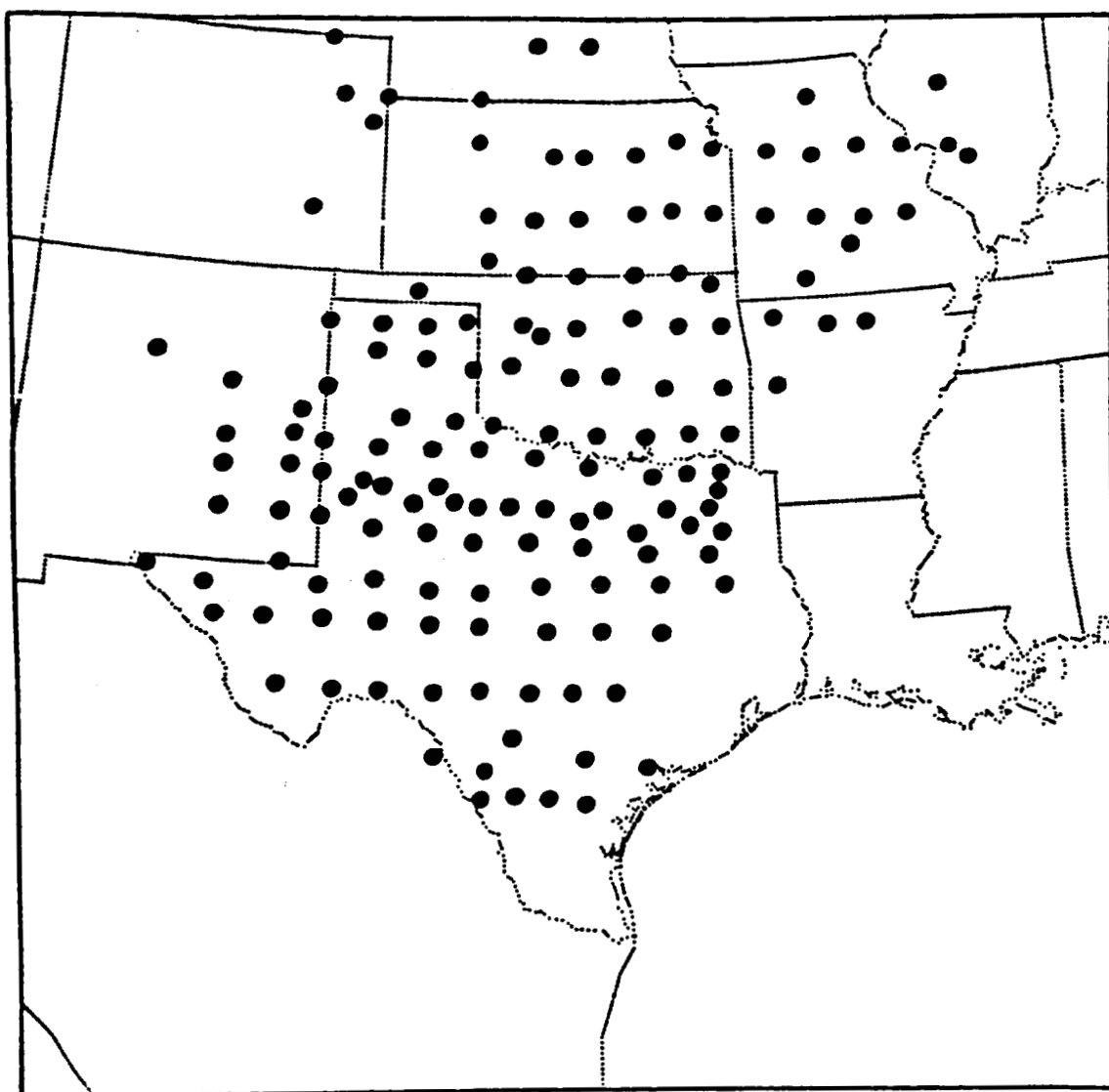
Figure 1   The VAS retrieval sites for 2330 GMT 6 March 1982.
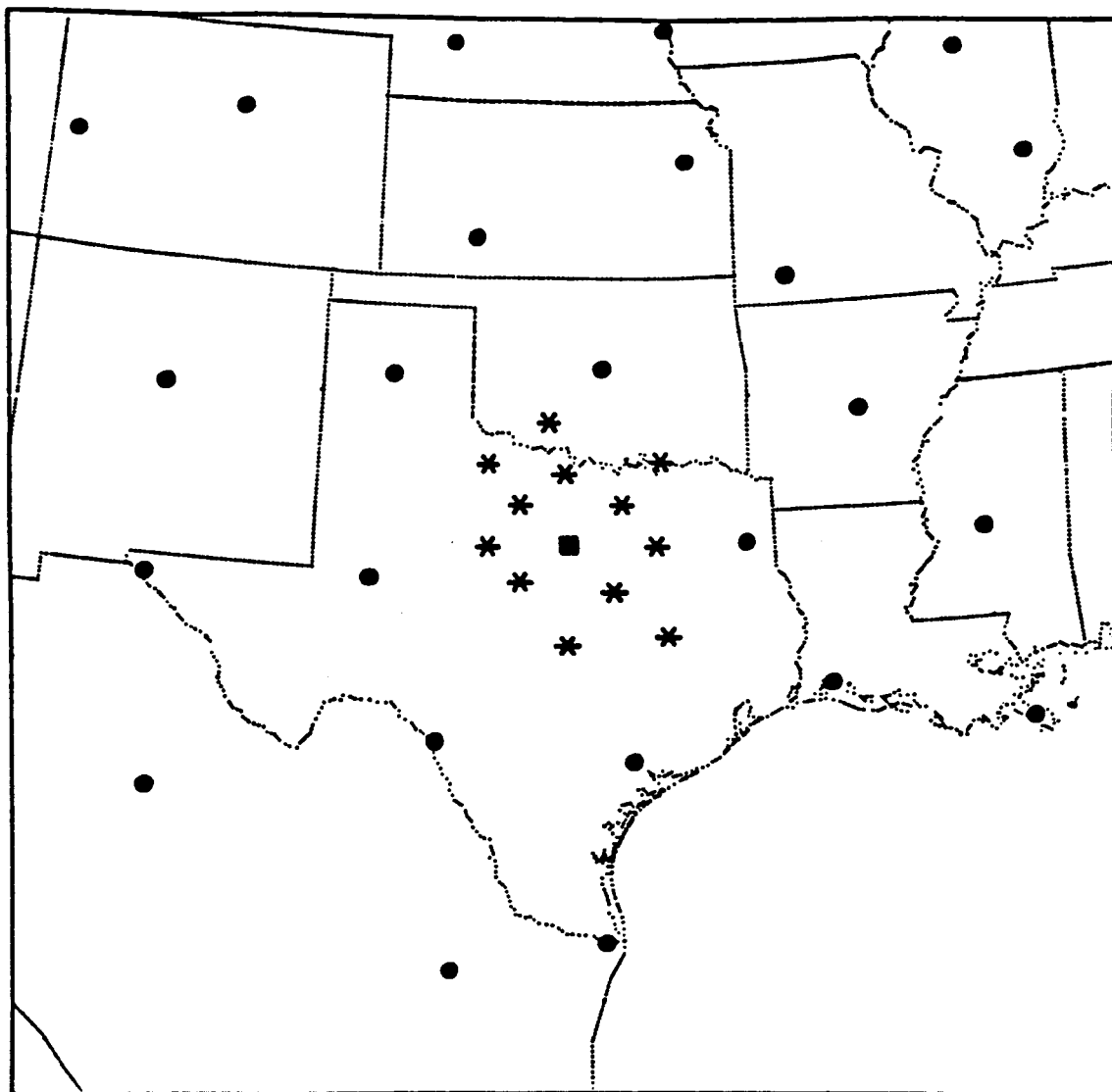
Figure 2   The rawinsonde observation locations for 0000 GMT
            7 March 1982. The locations of the special-network
            rawinsonde observations are shown by asterisks. The
            rawinsonde site at Stephenville, Texas is represented
            by a square. The locations of the NWS rawinsonde
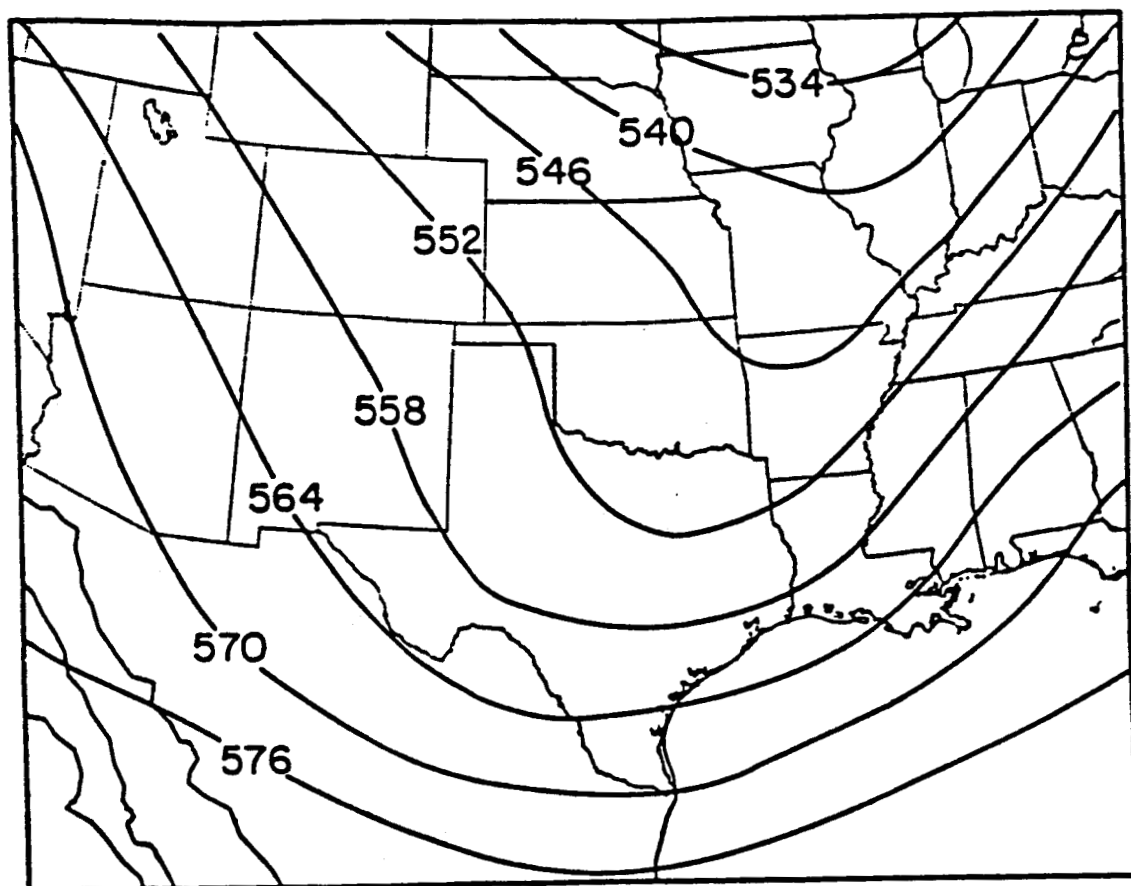   observations for the same time are represented by dots.

Figure 3   Regional NWS surface pressure analysis for 0000 GMT
            7 March 1982. Several representative surface observa-
            tions are plotted using the standard code.

Figure 4   The NWS 500-mb geopotential height analysis (decameters)
             for 0000 GMT 7 March 1982. The contour interval is 60m.
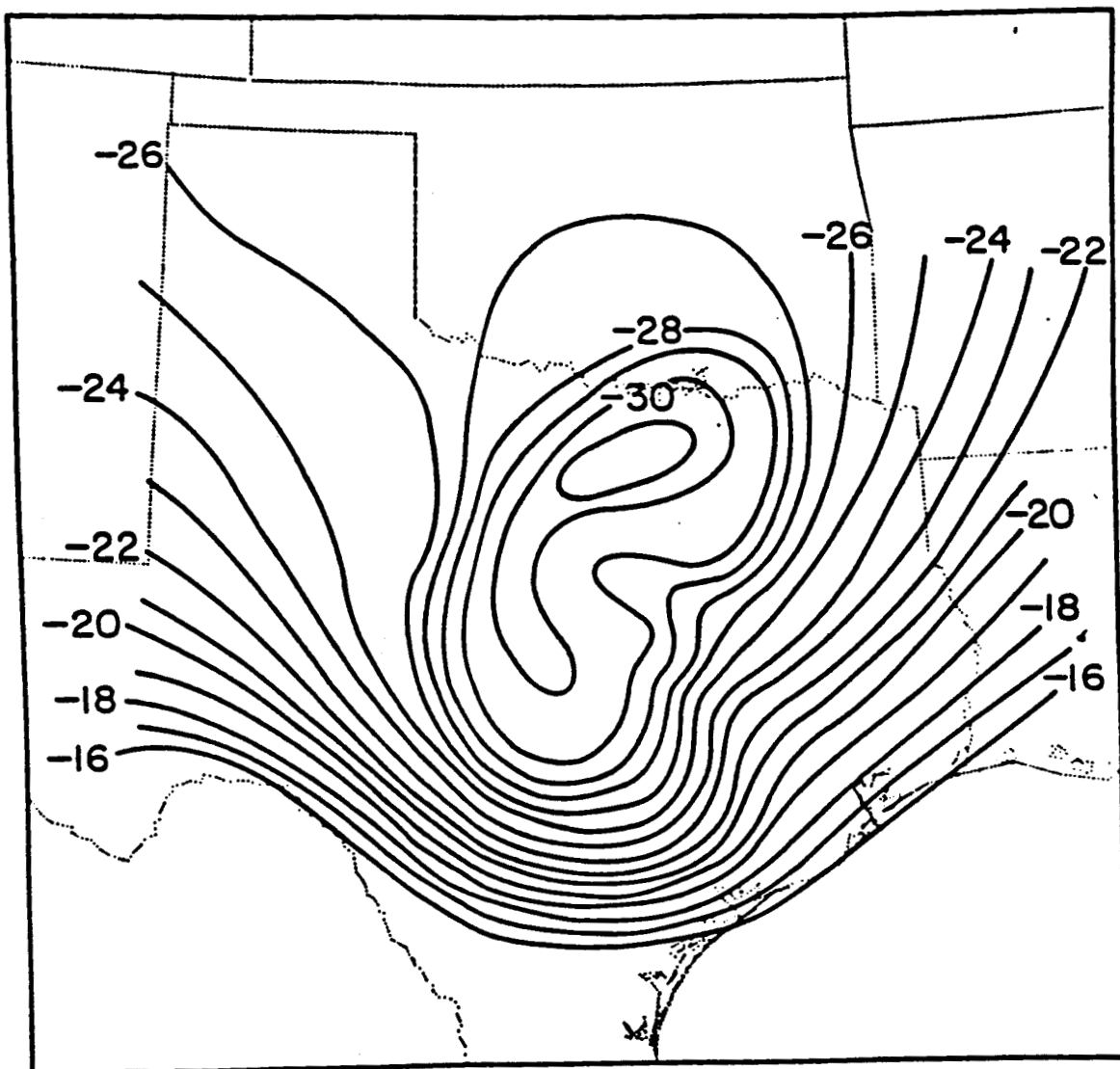
Figure 5   The 500-mb temperature subjective analysis (°C) for 0000 GMT 7 March 1982. The analysis is based on the special-network and surrounding NWS rawinsonde observations. The contour interval is 1°C.
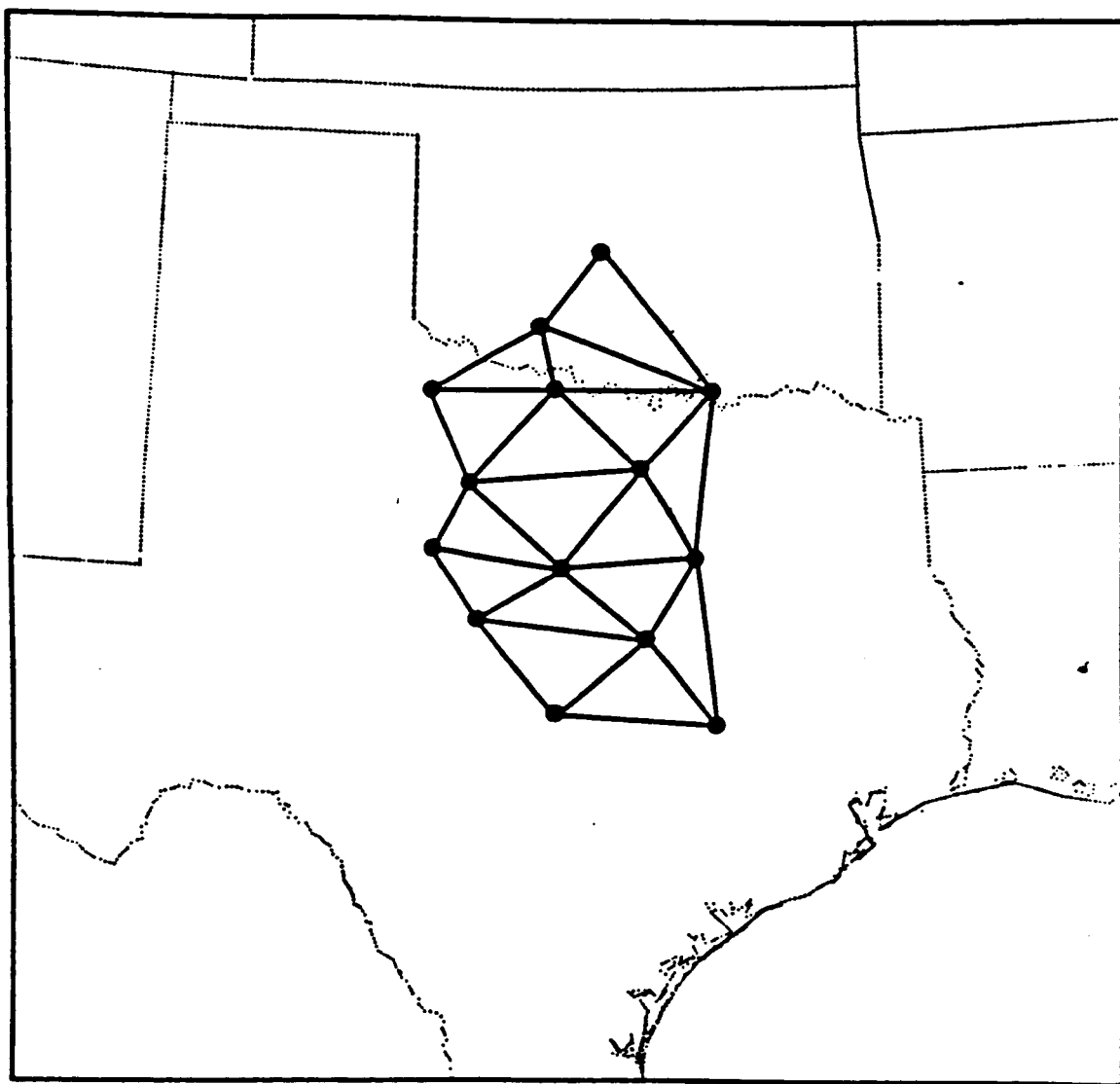
Figure 6   The combinations of observation points used to calculate
the horizontal first-derivative error.
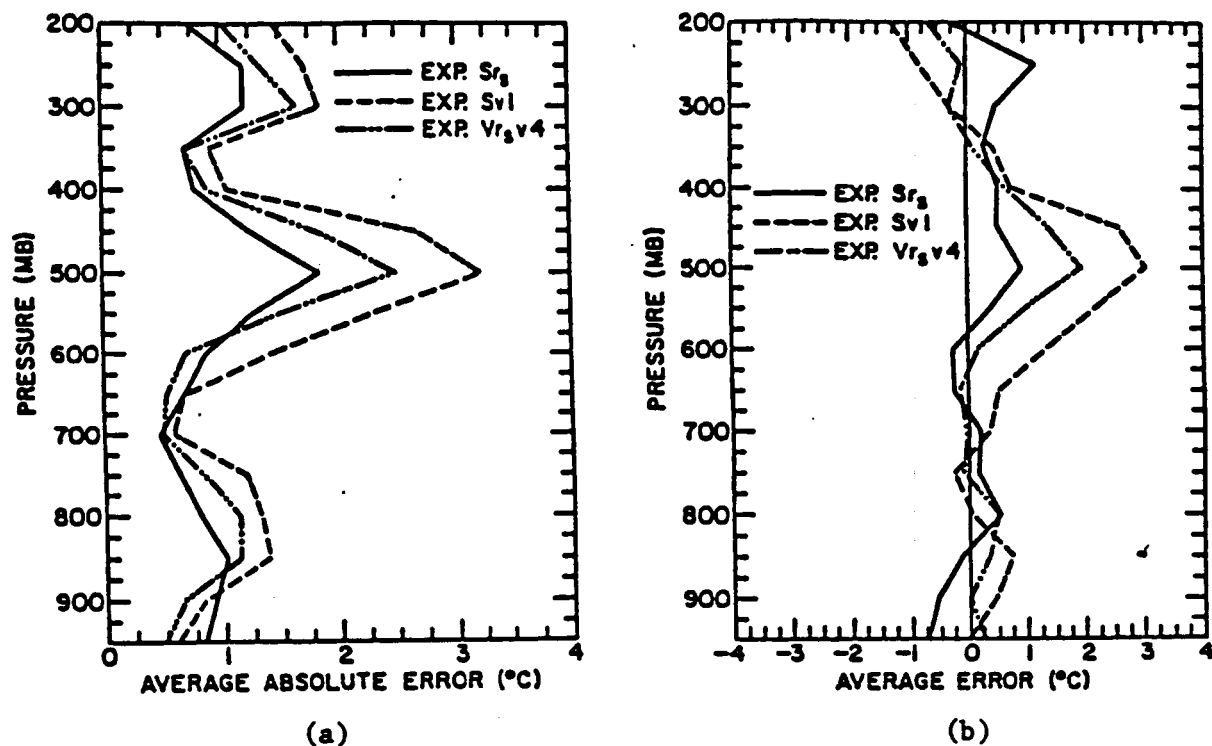
Figure 7   The temperature error statistics for the experiments Sr_s,
            Svl, and $Vr_s v4$.
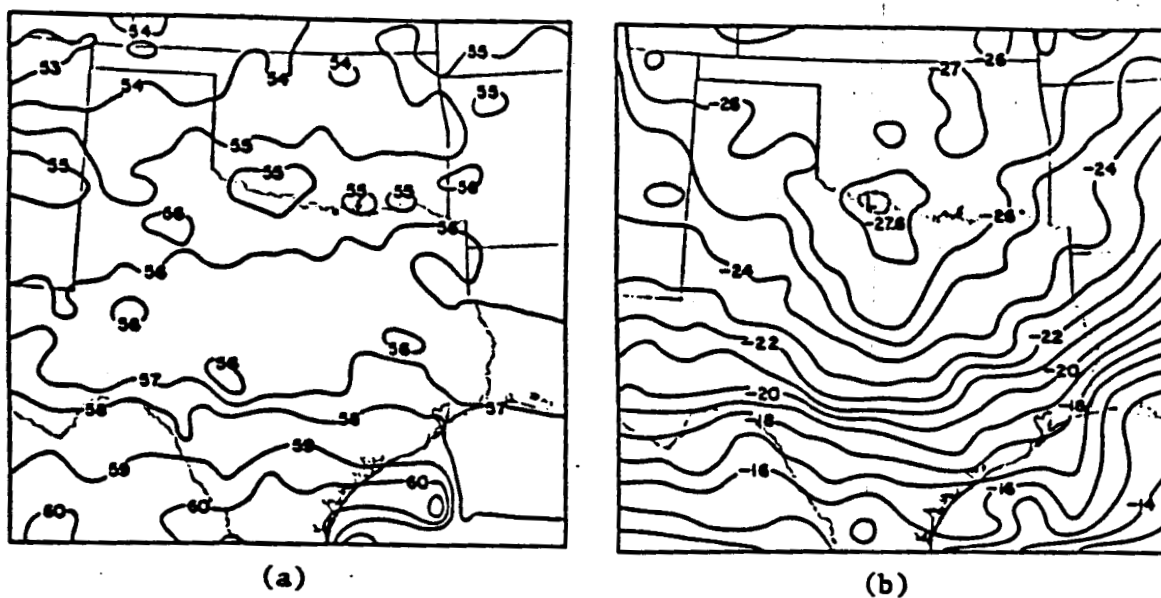   a.   Average absolute error
            b.   average error.

(a)

(b)
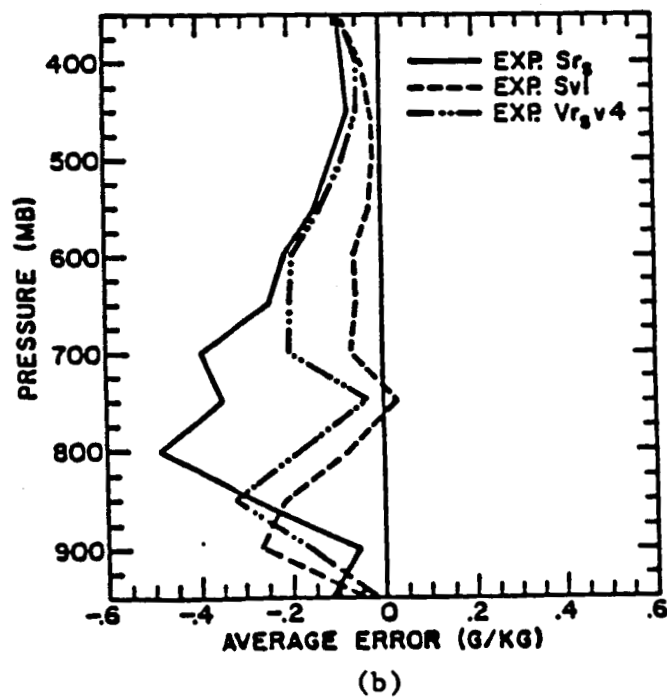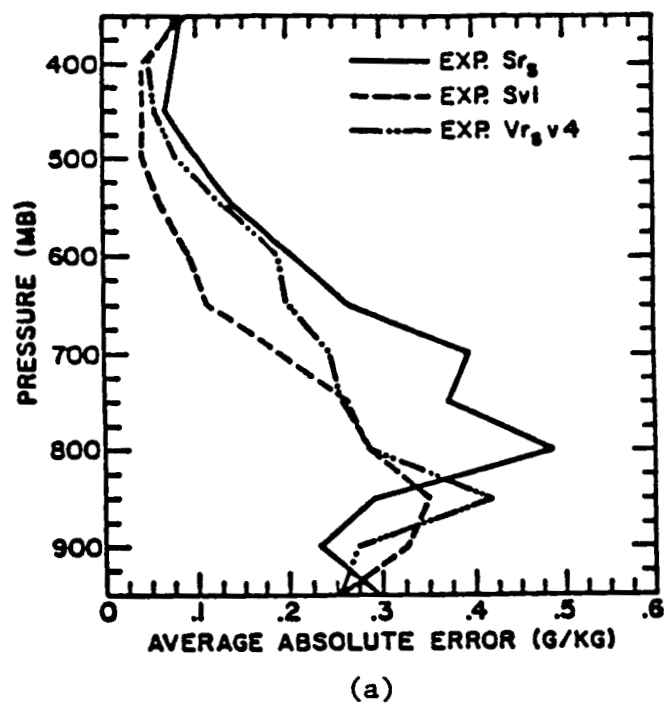
Figure 8   The mixing-ratio error statistics for experiments
            Sr_s, Svl, and Vr_sv4.
            a.   Average absolute error
            b.   Average error.

(a) (b)

Figure 9   The results of experiments $Vr_s v_r 2$ using rawinsonde data
           and VAS radiance data.
       a. Analysis of VAS channel-4 raw radiances (ergs).
           The contour interval is 1 erg.
       b. The 500-mb temperature analysis (°C) from
           experiment $Vr_s v_r 2$.   The contour interval is 1°C.
           The dashed contour in the region of the cold pocket
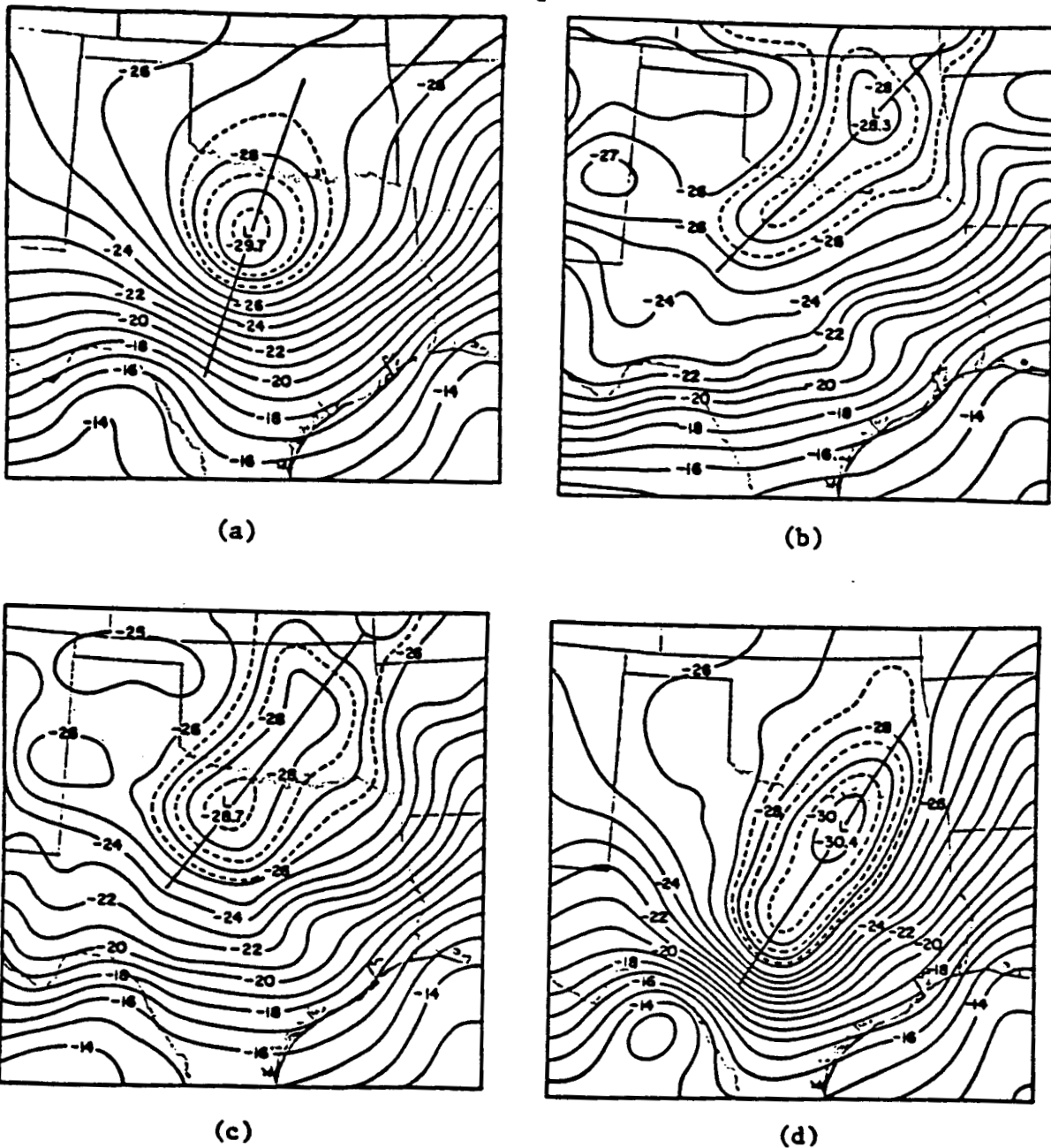   is plotted at a 0.5°C interval.

(a)

(b)

(c)

(d)

Figure 10   The 500-mb temperature analysis (°C) for Sr$_s$ (a), Srl (b), Vr$_s$v4 (c)
and the verification field (d). The contour interval is 1°C,
however the dashed contours in the region of the cold pocket are
plotted every 0.5°C. One-dimensional temperature plots were taken
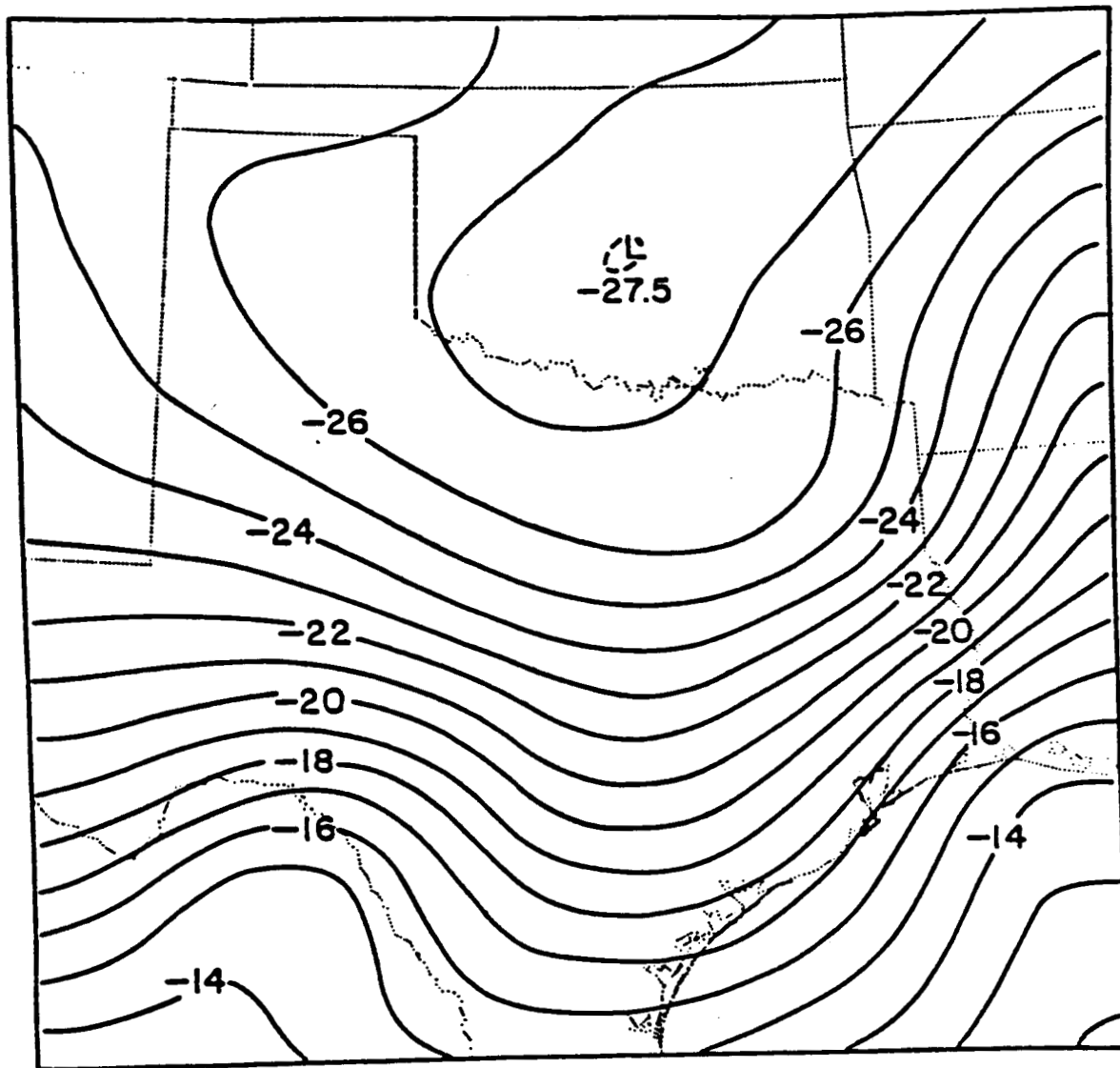along the lines indicated in each analysis.

Figure 11   The 500-mb temperature analysis (°C) from experiment Sr. The
contour interval is 1°C. The dashed contours in the region of
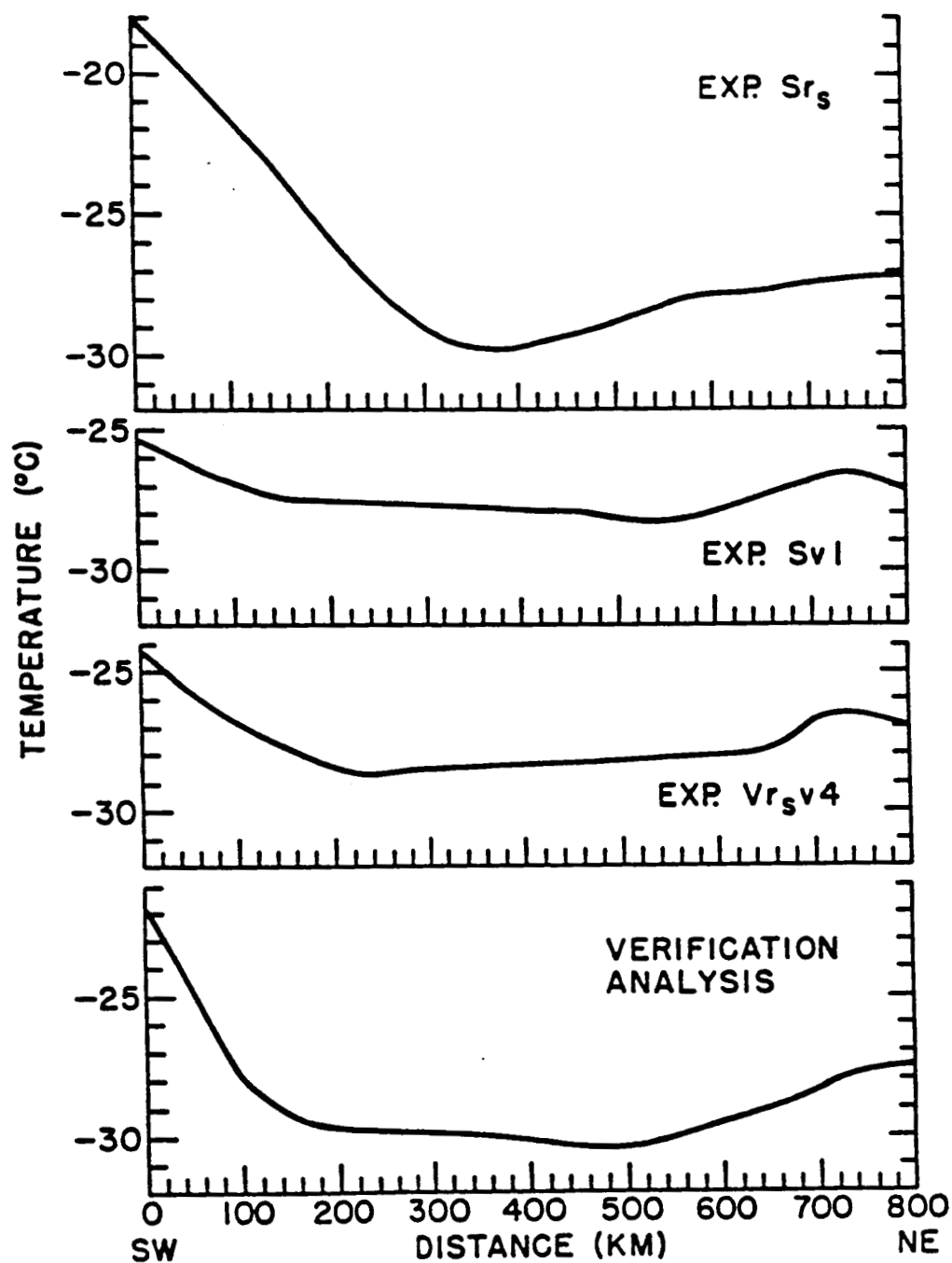the cold pocket are plotted every 0.5°C.

Figure 12   The one-dimensional 500-mb temperature plots for
experiments Sr_s, Sv1, Vr_sv4, and the analysis of
the special-network data and the NWS rawinsonde data.
The lines along which the data are plotted are shown
in Fig. 11.